Biomechanical comparison of mini-plate and screw fixation in minimally invasive distal metatarsal osteotomy for hallux valgus

a finite element and cadaveric study

From National Yang Ming Chiao Tung University, Taipei, Taiwan

Cite this article:
Bone Joint Res 2026;15(9): 1074–1087.

DOI: 10.1302/2046-3758.159.BJR-2026-0011.R1

Correspondence should be sent to Chun-Li Lin cllin2@nycu.edu.tw

Y-H. Chan,[1] Y-Y. Chen,[2] K-W. Chong,[3] C-H. Chu,[2] H-W. Wang,[1,4] S-F. Huang,[1,4] C-L. Lin[1,4]

[1]Department of Biomedical Engineering, National Yang Ming Chaio Tung University, Taipei, Taiwan
[2]Orthopedic Department, Show-Chwan Memorial Hospital, Chang Hua, Taiwan
[3]BJIOS Orthopaedics, Singapore, Singapore
[4]Medical Device Innovation and Translation Center, National Yang Ming Chaio Tung University, Taipei, Taiwan

Aims
To biomechanically compare the stability of mini-plate and dual-screw fixation following minimally invasive distal metatarsal osteotomy for hallux valgus, with an emphasis on early-stage stability under clinically relevant loading conditions.

Methods
Three fixation configurations were evaluated: mini-plate fixation with two (PS2) or three (PS3) locking screws and dual-screw fixation (DS). Finite element analysis (FEA) was performed to quantify displacement and stress distribution under controlled bending and torsional loading, providing insight into internal load transfer mechanisms not accessible experimentally. Fresh-frozen human cadaveric specimens then underwent distal chevron metatarsal osteotomy and fixation according to each configuration (n = 3 per group). Cyclic and static bending tests were performed to simulate early postoperative weightbearing, and displacement responses were recorded. FE predictions were compared with experimental displacement trends.

Results
Under bending loads, both FEA and cadaveric testing consistently demonstrated that PS3 exhibited the smallest displacement, followed by PS2, with DS showing the greatest instability. FE analysis further revealed that mini-plate fixation reduced bone stress at the osteotomy site but increased implant stress, whereas DS showed higher bone stress concentration. Under torsional loading, FE results indicated lower displacement but higher bone stress in DS. Cadaveric cyclic tests confirmed the superior stability of PS3, showing the least displacement accumulation over 1,000 cycles ($p < 0.05$). In static testing, PS3 achieved the highest failure load (~423 N), followed by PS2 (~248 N), while DS showed the lowest (~205 N).

Conclusion
Mini-plate fixation, particularly PS3, provides superior resistance to bending-induced micromotion compared with DS, with consistent agreement between FE predictions and experimental findings. FEA further elucidated internal stress distribution, highlighting increased bone stress concentrations in DS. Overall, mini-plate fixation offers a more stable and clinically reliable construct for maintaining correction during early postoperative weightbearing.

Article focus

- To biomechanically compare mini-plate and dual-screw fixation strategies following minimally invasive distal metatarsal osteotomy for hallux valgus.
- To evaluate early-stage fixation stability under clinically relevant bending-dominated loading conditions using finite element analysis (FEA) and cadaveric testing.
- To provide a structural mechanics-based explanation for differences in fixation performance under bending and torsional loads.

Key messages

- Mini-plate fixation demonstrated superior resistance to bending-induced micromotion compared with dual-screw fixation in distal metatarsal osteotomy.
- Finite element predictions under bending loads were consistent with cadaveric cyclic bending results, supporting the validity of numerical simulation for clinically dominant loading scenarios.
- Although dual-screw fixation showed favourable torsional resistance under idealized conditions, it was associated with higher bone stress concentrations, which may increase the risk of fixation-related complications.

Strengths and limitations

- This study combined FEA with fresh-frozen human cadaveric biomechanical testing, allowing complementary evaluation of fixation stability under controlled and clinically representative loading conditions.
- Structural mechanics concepts, including the second moment of area and polar moment of inertia, were applied to provide a mechanistic explanation for observed biomechanical differences.
- Limitations include a relatively small sample size and the use of idealized material assumptions in the finite element models; isolated torsional loading could not be reproduced in physical specimens.

Introduction

Minimally invasive surgery (MIS) for hallux valgus correction has advanced rapidly in recent years.[1-6] Among MIS techniques, modified distal first metatarsal osteotomy – such as the minimally invasive chevron and Akin technique – combined with screw fixation has emerged as a representative approach, emphasizing small incisions, reduced soft-tissue disruption, and accelerated postoperative recovery.[5,7-13] Nevertheless, clinical reports continue to document complications, including dorsal angular deformity of the distal fragment, micromotion at the osteotomy interface, and fixation failure, particularly in patients subjected to early weightbearing or those with compromised bone quality.[11,14,15] These observations suggest that the mechanical stability of the post-osteotomy fixation construct remains a critical determinant of surgical success.[16]

Currently, fixation strategies following minimally invasive distal metatarsal osteotomy predominantly rely on screw-based constructs, including three-point fixation based on the concept of multicortical anchoring and dual-screw configurations incorporating proximal intramedullary orientation.[12-18] By increasing screw–cortical bone contact, these methods are theoretically intended to enhance osteotomy stability and are widely adopted because of their minimally invasive nature. However, screw fixation typically requires proximal screw insertion via additional skin incision, and depends on fluoroscopic guidance and dedicated targeting devices to achieve optimal insertion angles and cortical engagement, thereby imposing technical demands and a non-trivial learning curve.[18] Moreover, because the screws are primarily distributed near the neutral axis of the osteotomy construct, their capacity to resist dorsal angular deformation and to control micromotion at the osteotomy interface under repetitive bending loads may be inherently limited.[19,20] Consequently, the mechanical behaviour of these fixation configurations warrants further systematic investigation.[21,22]

With ongoing miniaturization of implants and advancements in surgical techniques, recent studies have introduced the concept of mini-plate fixation applied through a distal osteotomy soft-tissue window.[23] This approach enables fixation without requiring additional proximal incisions or requiring positioning or targeting devices, thereby potentially simplifying the surgical procedure. Accordingly, under identical osteotomy geometry and loading conditions, whether a mini-plate inserted through a distal window with lateral screw fixation can provide quantifiable mechanical advantages in terms of bending stiffness and control of angular deformation remains an open question and warrants further investigation.

From a biomechanical perspective, the primary functional load acting on a distal chevron osteotomy of the first metatarsal arises from forefoot and hallux flexion–extension during the toe-off phase of gait, generating a bending moment predominantly characterized by sagittal-plane bending.[24,25] However, during turning and non-linear movements or in the presence of external perturbations, the osteotomy region may also be subjected to axial torsional loading of the hallux. Notably, most existing biomechanical studies have focused primarily on flexion–extension or unidirectional bending loads, with comparatively limited attention given to the combined effects of bending and torsion across different fixation configurations.[26,27] This imbalance is partly attributable to the technical challenges associated with reliably applying controlled pure torsional loads in macroscopic experimental setups.

Therefore, this study aims to establish a comprehensive mechanical evaluation framework integrating numerical simulation and experimental validation to compare the stability performance of different fixation strategies following distal first metatarsal chevron osteotomy. Finite element analysis (FEA) was performed using a standardized osteotomy model to evaluate three implant fixations: 1) mini-plate fixation with two laterally oriented locking screws (PS2); 2) mini-plate fixation with three laterally oriented locking screws (PS3); and 3) a percutaneous dual-screw configuration with three-point fixation (DS). For each configuration, osteotomy fragment displacement and stress distribution were systematically assessed under bending and axial torsional loading conditions. Subsequently, based on the numerical findings, cyclic bending biomechanical tests were conducted using fresh-frozen human cadaveric foot specimens, focusing on clinically dominant bending loads to experimentally validate the FEA predictions under bending moment conditions. By integrating FEA with biomechanical experimentation, this study seeks to delineate the mechanical advantages and limitations of different fixation strategies under primary clinical loading mechanisms, while further exploring potential risks under atypical torsional scenarios through numerical simulation. The results aim to provide a robust biomechanical basis for optimizing fixation strategy selection following minimally invasive hallux valgus osteotomy.

Methods

Solid model generation of the osteotomy and implant fixations

The left first metatarsal bone of a 62-year-old male donor (No. 2 in Table I) was used as the basis for model construction. CT images were acquired and used to generate a 3D geometrical model. The CT slice interval was set to 0.625 mm to ensure sufficient spatial resolution for accurate reconstruction of the first metatarsal anatomy. Image processing was performed to segment the cortical and cancellous bone contours. Reverse engineering software (Geomagic Design, USA) was subsequently employed to reconstruct the 3D geometry and perform surface smoothing. The finalized 3D model was then imported into computer-aided design software (SpaceClaim, USA) to simulate the distal chevron osteotomy and to construct the various implant fixation configurations.

Based on the distal metatarsal osteotomy technique commonly employed in minimally invasive hallux valgus correction, a standardized transverse osteotomy was created at 2.4 cm proximal to the distal end of the first metatarsal (Figure 1a). The distal fragment was subsequently translated 7 mm laterally to establish a standardized metatarsal osteotomy model (Figure 1b).

Three different implant fixations were developed for comparative analysis. The first configuration consisted of mini-plate fixation using the plate system (PS) (Spear Locking Plate I and II; A Plus Biotechnology Co., Taiwan). This mini-plate with 2 mm thickness is designed to be inserted through the distal osteotomy soft-tissue window in an intramedullary position along the inner medial cortical surface of the first metatarsal. According to the number of locking fixation screws, two plate-based models were defined: PS2, in which one locking screw (2.4 mm in diameter and 26 mm in length) was placed at both the proximal and distal sides of the osteotomy, and PS3, which incorporated three locking screws (2.7 mm in diameter and 24 mm in length) – two at the distal fragment and one at the proximal fragment (Figure 1b, left and middle).

The second fixation strategy was a screw-based configuration (DS), employing two screws (4.1 mm diameter headless screw; A Plus Biotechnology Co.) with different orientations. The first screw was inserted from the medial cortex of the proximal first metatarsal and advanced distally along the longitudinal axis in an oblique intramedullary orientation. This screw was anchored exclusively within the proximal fragment without penetrating the lateral cortex, thereby providing internal support and resistance to bending. The second screw followed a three-point fixation concept, sequentially engaging the medial and lateral cortices of the proximal fragment and anchoring into the distal fragment, with the aim of enhancing interfragmentary stability and controlling displacement at the osteotomy interface (Figure 1b, right).

All implant geometries were constructed within a computer-aided design environment. The osteotomy models and corresponding implant fixation positions were then combined using Boolean operations to generate the complete solid models of the three metatarsal osteotomy fixation constructs for subsequent numerical analysis (Figure 1b).

Finite element analysis

Three metatarsal osteotomy implant fixation constructs were imported into FEA software (ANSYS, v21.1; ANSYS Inc., USA) to establish the corresponding FE models. All models were meshed using quadratic ten-node tetrahedral elements (Figure 1c). A mesh convergence test was conducted using five element sizes (1.0, 0.9, 0.8, 0.7, and 0.5 mm). The mesh was progressively refined, and the average displacement of the distal osteotomy segment was evaluated. When the mesh size reached 0.5 mm, the variation in displacement was less than 5%, indicating that mesh convergence had been achieved (Table II). Therefore, a mesh size of approximately 0.5 mm was adopted for subsequent analyses.

Material properties were assigned based on relevant literature and all materials – including cortical bone, cancellous bone, and titanium alloy used for plates and screws – were assumed to be homogeneous, isotropic, and linearly elastic.[28,29] The elastic modulus and Poisson's ratio for each material are listed in Table III. Nonlinear frictional contact element was used to mimic the adaption at the osteotomy interface with a coefficient of friction of 0.45, consistent with previously reported biomechanical studies.[26] The proximal end of the first metatarsal was fully constrained in all degrees of freedom to represent the stabilizing effect of the proximal midfoot during forefoot loading.

Two loading conditions were applied to each FE model. In the first condition, a 100 N vertical downward force was applied to the distal osteotomy fragment to simulate the bending moment generated during forefoot and hallux flexion–extension (Figure 1d). In the second condition, a torsional moment of 500 N/mm was applied to the distal fragment to simulate axial torsion of the hallux (Figure 1e). In both loading scenarios, a small axial preload of 10 N was applied across the osteotomy interface to maintain contact stability and prevent numerical separation, without substantially influencing the overall deformation response.[26,30]

For each fixation configuration and loading condition, the total displacement of the distal metatarsal fragment, the maximum von Mises stress, and its spatial distribution in both the implant and bone, as well as the maximum (ε_1) and minimum (ε_3) principal strains of the bone, were recorded for subsequent comparison.

Specimen preparation and surgical technique for human cadaveric study

Nine freshly frozen human cadaveric foot specimens (nine feet) were used, with a mean age at death of 68 years (SD 10.83, five males and four females) (Table I). All specimens were visually inspected and radiologically screened to exclude gross deformity, fracture, or prior surgical intervention. The first metatarsal length, metatarsal head width, hallux valgus angle, and intermetatarsal angle were measured, yielding

Table I. Specimen demographic details, physical description, and experiment randomization.

No.	Left/right	Age, yrs	Sex	Osteotomy displacement, mm	First metatarsal length, mm	Metatarsal head width, mm	HVA/IMA, °	Fixation type
1	L	49	F	8.39	61.2	21.1	11.4/4.1	PS2
2	L	62	M	6.65	69.4	21.4	10.5/3.6	PS2
3	L	81	M	7.13	62.4	18.9	11.4/2.8	PS2
4	L	81	M	7.28	63.8	20.0	12.6/6.6	PS3
5	L	72	M	7.49	63.5	16.6	11.8/5.8	PS3
6	R	79	M	8.16	56.4	19.2	7.9/2.7	PS3
7	L	64	F	6.72	60.0	19.2	5.2/5.6	DS
8	L	63	F	6.55	54.5	16.2	4.1/8.5	DS
9	R	63	F	7.76	54.1	17.6	10.0/9.0	DS
Mean	N/A	68	N/A	7.35	60.6	18.9	9.4/5.4	N/A

DS, dual-screw fixation; F, female; HVA, hallux valgus angle; IMA, intermetatarsal angle; L, left; M, male; N/A, not applicable; PS2, mini-plate fixation with two locking screws; PS3, mini-plate fixation with three locking screws; R, right.

mean values of 9.5° (SD 3.03°) and 5.4° (SD 2.32°) for hallux valgus angle and intermetatarsal angle, respectively.

Specimens were thawed at room temperature (approximately 25°C) for 24 hours prior to surgery and kept moist with continuous saline irrigation throughout preparation and fixation. A standardized minimally invasive distal first metatarsal chevron osteotomy was performed in all specimens by an experienced foot and ankle surgeon under fluoroscopic guidance. A 3 mm skin incision was made medial to the first metatarsal neck, and a transverse osteotomy was created using a Shannon burr, oriented approximately 15° relative to the long axis of the metatarsal in the sagittal plane.

After completion of the osteotomy, the distal fragment was translated laterally by approximately 7 mm to simulate a clinically representative correction. Specimens were then randomly allocated to three fixation groups (n = 3 per group): PS2, PS3, and DS. The cadaveric fixation strategies were designed to reflect the three representative configurations evaluated in the FEA, while allowing for standard clinical implantation under fluoroscopic guidance.

In the PS2 and PS3 groups, the same specifications as FE analysis were inserted through the distal osteotomy window and positioned along the intramedullary aspect of the medial cortical surface of the first metatarsal. Two or three laterally oriented locking screws were inserted obliquely through the plate, anchoring into the proximal and distal cortical segments.

In the DS group (the same specifications in FE analysis), fixation was achieved using two obliquely oriented screws: one proximally inserted intramedullary screw for axial support and one three-point fixation screw crossing the osteotomy to enhance interfragmentary stability. All screws were inserted under fluoroscopic guidance to ensure consistent positioning and to avoid unintended cortical penetration. An Akin osteotomy was intentionally not performed to avoid confounding the biomechanical behaviour of the first metatarsal. Final fluoroscopic images were obtained to confirm osteotomy displacement, fixation configuration, and implant positioning prior to biomechanical testing.

Biomechanical cyclic bending testing

Following osteotomy and fixation, all foot specimens were surgically prepared by removing surrounding soft tissues and adjacent skeletal structures, retaining only the repaired first metatarsal as the test specimen. The proximal base of the first metatarsal was embedded in an epoxy resin, with a uniform embedding depth of 30 mm measured proximally from the osteotomy plane. This standardized embedding depth ensured consistent lever arm length and loading conditions across all specimens. The embedding technique provided rigid fixation and effectively minimized unintended displacement caused by clamp slippage or deformation, thereby ensuring that the applied loads acted primarily on the osteotomy site and fixation construct.

All specimens were tested using a cantilever configuration, with the first metatarsal inclined at 15° relative to the horizontal plane to simulate the anatomical orientation and loading direction of the first metatarsal during the standing and toe-off phases of gait (Figure 2). This experimental setup has been widely adopted in biomechanical studies of first metatarsal osteotomies, as it effectively reproduces the bending moment generated by ground reaction forces acting on the metatarsal head and allows evaluation of fixation stability under repetitive bending loads.[10,19,20,31]

Prior to testing, all specimens were wrapped in saline-soaked gauze and stored at 20°C. They were subsequently thawed at room temperature (approximately 25°C) for a minimum of 12 hours to minimize potential alterations in material properties associated with cryopreservation. Each specimen was then mounted on an all-electric material testing system (Instron E3000, Instron, USA) equipped with custom fixtures, a load frame, and force transducers. Cyclic loading and failure testing were performed to simulate fatigue behaviour induced by repetitive weightbearing during the early postoperative gait period.

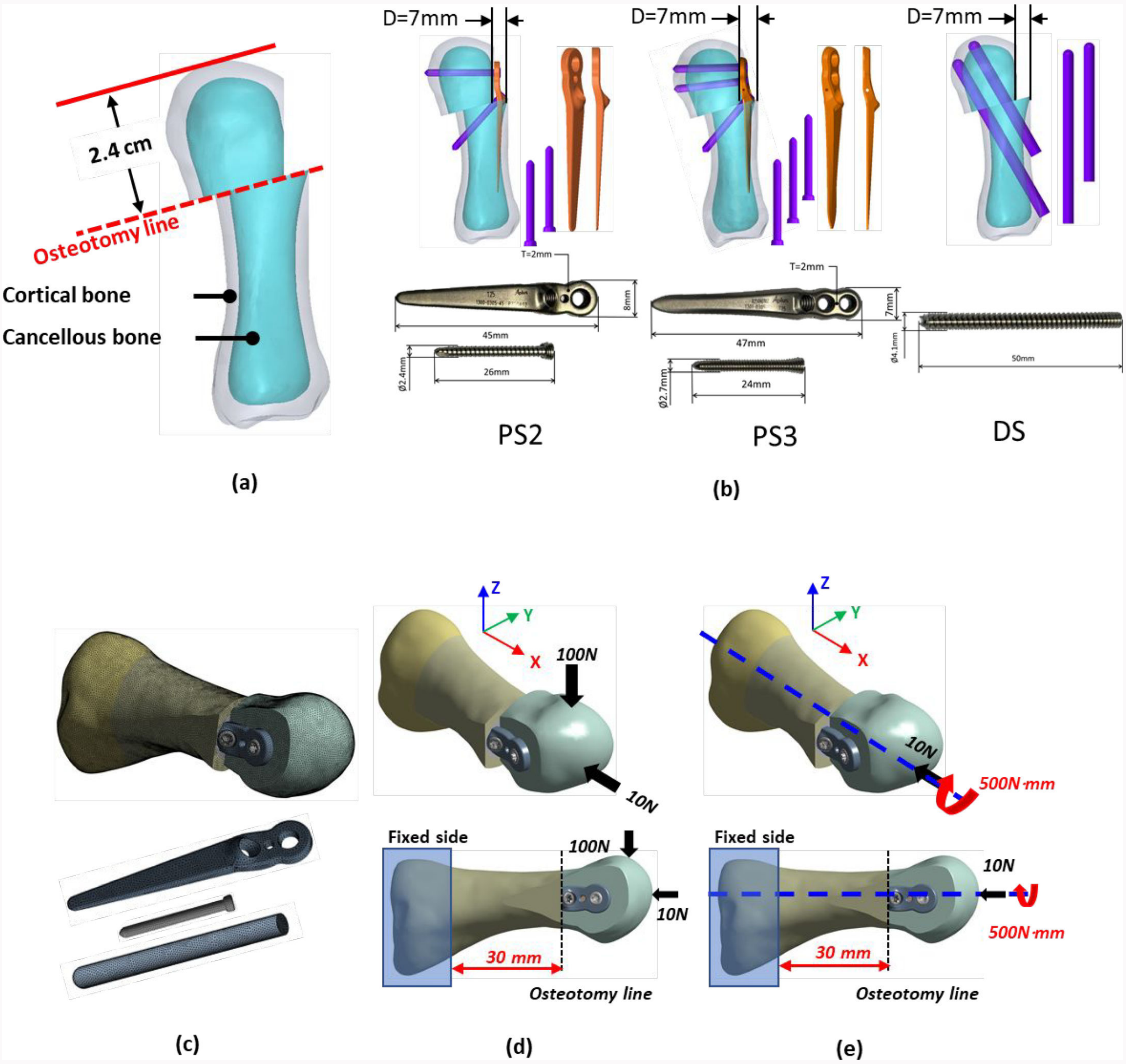

Fig. 1

Finite element model construction and fixation configurations. a) Standardized distal chevron osteotomy model of the first metatarsal created based on CT data. b) Three fixation configurations evaluated in this study. Left: mini-plate fixation with two locking screws (PS2); middle: mini-plate fixation with three locking screws (PS3); and right: dual-screw fixation (DS). c) Finite element mesh of the osteotomy–implant construct. Boundary conditions and loading setup for d) bending and e) torsional simulations. D, distance.

Table II. Mesh convergence analysis showing that further mesh refinement results in negligible changes, confirming mesh-independent results.

	0.5 mm			0.7 mm			0.8 mm			0.9 mm			1.0 mm			Error
System	Node #	Element #	Dis., mm	Node #	Element #	Dis., mm	Node #	Element #	Dis., mm	Node #	Element #	Dis., mm	Node #	Element #	Dis., mm	
PS2	1,034,392	723,732	0.238	576,665	401,143	0.242	354,537	244,646	0.243	269,778	184,962	0.245	211,952	144,582	0.246	1.55%
PS3	1,043,551	730,723	0.219	491,076	341,228	0.226	356,987	246,727	0.228	269,741	185,199	0.230	212,694	145,369	0.234	2.86%
DS	1,063,635	741,972	0.220	501,283	347,180	0.229	363,949	250,789	0.231	275,167	188,529	0.234	215,281	147,027	0.236	4.35%

Dis., displacement; DS, dual-screw fixation; PS2, mini-plate fixation with two locking screws; PS3, mini-plate fixation with three locking screws.

During cyclic loading, a plantar-to-dorsal bending force was applied to the metatarsal head. Each specimen was subjected to a maximum of 1,000 loading cycles or until mechanical failure occurred. The loading range was set from 0 N to 31 N, corresponding to approximately one-third of the mean ultimate failure load of the first metatarsal osteotomy fixation constructs.[12,19,27] This load magnitude has been validated in previous forefoot osteotomy biomechanical

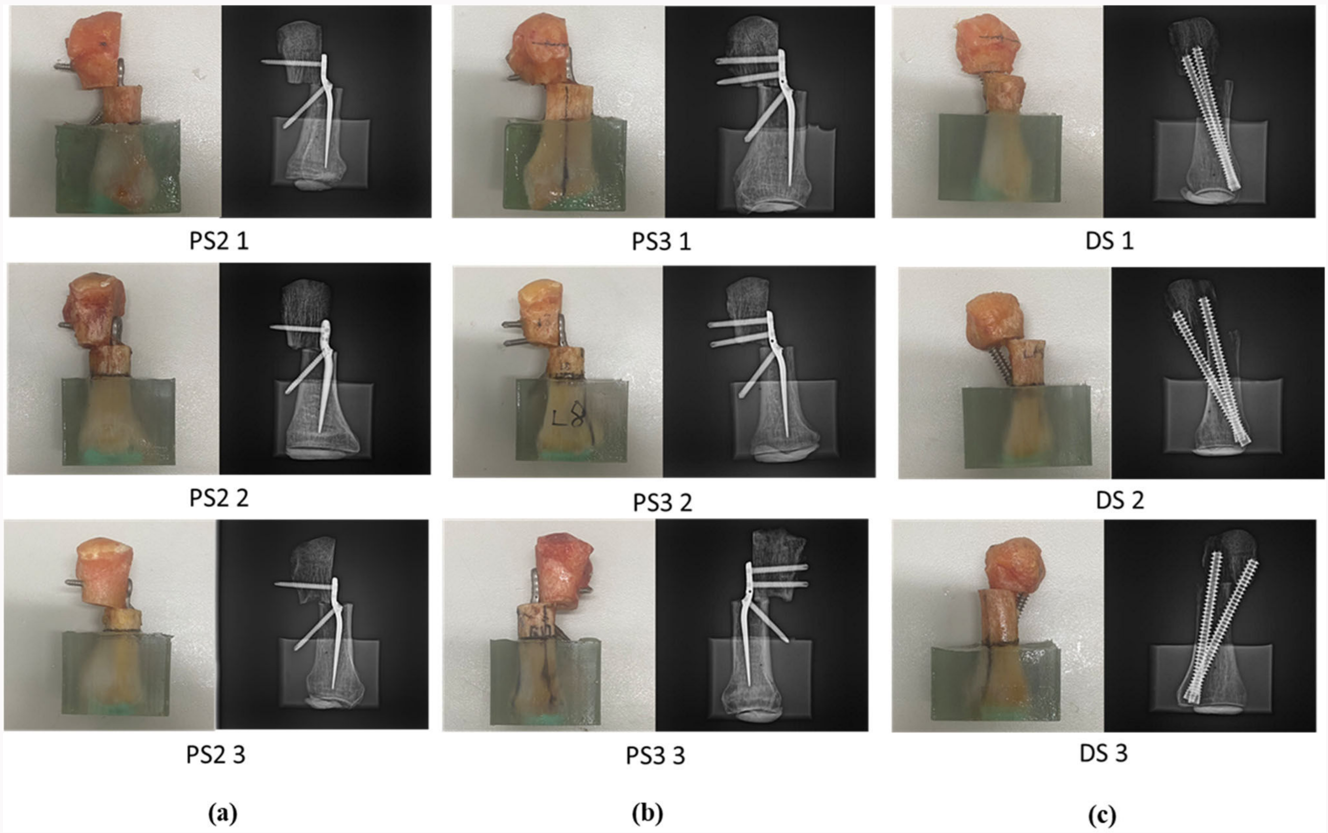

Fig. 2
Biomechanical cyclic bending test setup. Schematic illustration of the cantilever-based cyclic bending configuration used for gross biomechanical testing. The first metatarsal was fixed proximally and inclined at 15° relative to the horizontal plane to simulate the anatomical posture and bending moment experienced during the toe-off phase of gait. a) PS2 (mini-plate fixation with two locking screws) specimens 1 to 3. b) PS3 (mini-plate fixation with three locking screws) specimens 1 to 3. c) DS (dual-screw fixation) specimens 1 to 3.

Table III. Finite element mesh characteristics and material properties used in this study.

Variable	Plate and screw	Cortical	Cancellous	Reference
Elastic modulus, MPa	110,000	7,300	1,000	28
Poisson's ratio	0.3	0.3	0.3	29

studies as sufficient to challenge bending stability without inducing premature catastrophic failure. Cyclic loading was applied as a sinusoidal waveform at a frequency of 0.5 Hz, and 1,000 cycles were considered representative of repetitive loading experienced during a single day of early postoperative ambulation. Failure was defined as the occurrence of any of the following conditions prior to the completion of 1,000 cycles: 1) displacement at the osteotomy site exceeding 10 mm; 2) a sudden reduction in load-carrying capacity to less than 75% of the peak applied load; 3) screw loosening or fracture; or 4) fracture occurring at the screw entry site or within the osteotomy region. Upon failure, the number of cycles to failure and the corresponding failure mode were recorded.[12,19,20,32]

Specimens that successfully completed 1,000 loading cycles were further evaluated by quantifying their displacement responses under cyclic loading. After completion of the fatigue test, each specimen was subjected to a static compressive load applied at a constant displacement rate of 5 mm/s until failure. Failure was defined as a reduction in load exceeding 20%, at which point the test was terminated. The maximum load at failure and the corresponding failure modes were recorded for each fixation group.

Statistical analysis

Statistical comparisons among fixation groups were performed using the Kruskal–Wallis test with SPSS software (SPSS v. 22, IBM, USA). A p-value of < 0.05 was considered statistically significant.

Results

All specimens successfully underwent the planned osteotomy and fixation procedures. Fluoroscopic evaluation confirmed appropriate implant positioning, screw orientation, cortical engagement, and osteotomy alignment in all groups, consistent with the predefined surgical design (Figure 3). No implant malposition, cortical breach, or fixation failure was observed prior to biomechanical testing.

Under bending loading, the FE model demonstrated that PS3 exhibited the smallest displacement (0.288 mm), followed by PS2 (0.347 mm), whereas DS showed the largest displacement (0.408 mm). Under torsional loading, DS showed the smallest displacement (0.093 mm), followed by PS3

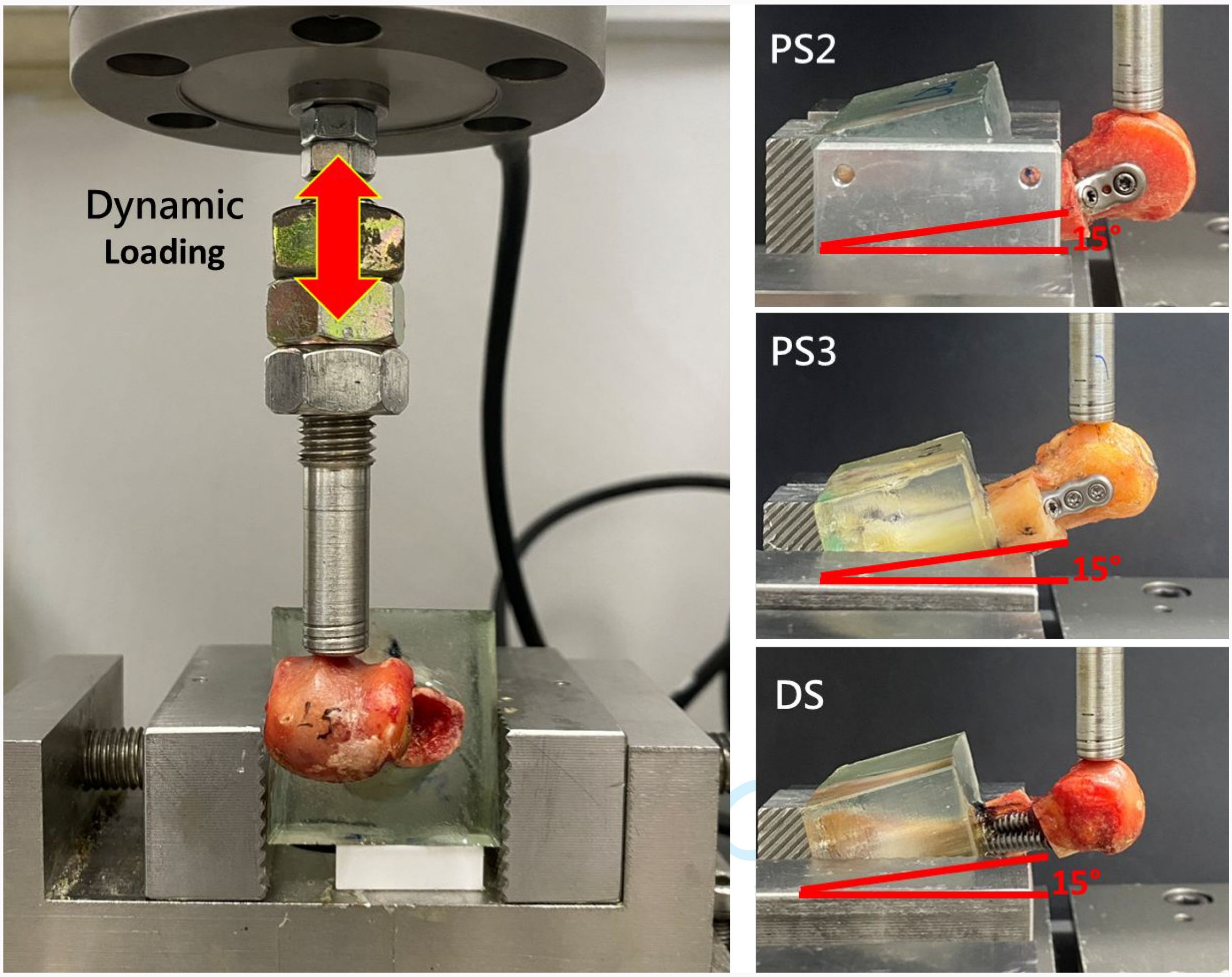

Fig. 3
Specimen preparation and fixation verification. Representative photographs demonstrating the three fixation strategies following minimally invasive distal metatarsal osteotomy: PS2 (mini-plate fixation with two locking screws); PS3 (mini-plate fixation with three locking screws); DS (dual-screw fixation). The radiograph images in Figure 2 confirm appropriate implant positioning, screw orientation, cortical engagement, and osteotomy alignment consistent with the experimental design.

(0.174 mm) and PS2 (0.220 mm). Stress analysis under bending revealed that the maximum bone stress was highest in the DS configuration (56.86 MPa), whereas PS2 and PS3 showed lower values (34.63 MPa and 35.12 MPa, respectively). In contrast, implant stress was highest in PS3 (680.46 MPa), followed by PS2 (252.74 MPa) and DS (126.47 MPa) (Figure 4). Under torsional loading, DS exhibited lower implant stress but higher bone stress compared with plate-based constructs (Figure 5).

For bone strain evaluation, the ε_1 followed the trend DS (3,354 $\mu\varepsilon$) > PS3 (1,706 $\mu\varepsilon$) > PS2 (1,643 $\mu\varepsilon$), while the ε_3 followed PS2 (–2,848 $\mu\varepsilon$) > PS3 (–2,474 $\mu\varepsilon$) > DS (–1,877 $\mu\varepsilon$) under bending loading (Figure 4). Under torsional loading, ε_1 followed DS (1,868 $\mu\varepsilon$) > PS2 (1,208 $\mu\varepsilon$) > PS3 (858 $\mu\varepsilon$), while ε_3 followed DS (–1,571 $\mu\varepsilon$) > PS2 (–1,226 $\mu\varepsilon$) > PS3 (–1,224 $\mu\varepsilon$) (Figure 5).

All fixation constructs demonstrated an initial increase in displacement during the early loading phase, followed by a gradual stabilization trend. After 1,000 loading cycles, PS3 showed the lowest displacement (0.255 mm), followed by PS2 (0.390 mm), while DS demonstrated the greatest displacement (0.688 mm) (Figure 6). Statistical analysis indicated no significant difference between PS3 and PS2 ($p > 0.05$), whereas both plate-based groups showed significantly lower displacement compared with the DS group ($p < 0.05$).

Distinct failure modes were observed among the fixation configurations. In the PS2 group, failure was characterized by rotation and gap opening at the osteotomy site. In the PS3 group, minimal displacement was observed prior to failure, with preservation of interfragmentary contact. In the DS group, failure predominantly occurred as bone fracture adjacent to the osteotomy region (Figure 7). The maximum failure load was highest in PS3 (≈ 423 N), followed by PS2 (≈ 248 N) and DS (≈ 205 N).

A consistent displacement trend was observed between FE predictions and experimental results under bending loading. In both analyses, PS3 exhibited the smallest displacement, followed by PS2, while DS demonstrated the greatest displacement.

Discussion

DS fixation is an established method for internal fixation following distal metatarsal osteotomy and is widely adopted in

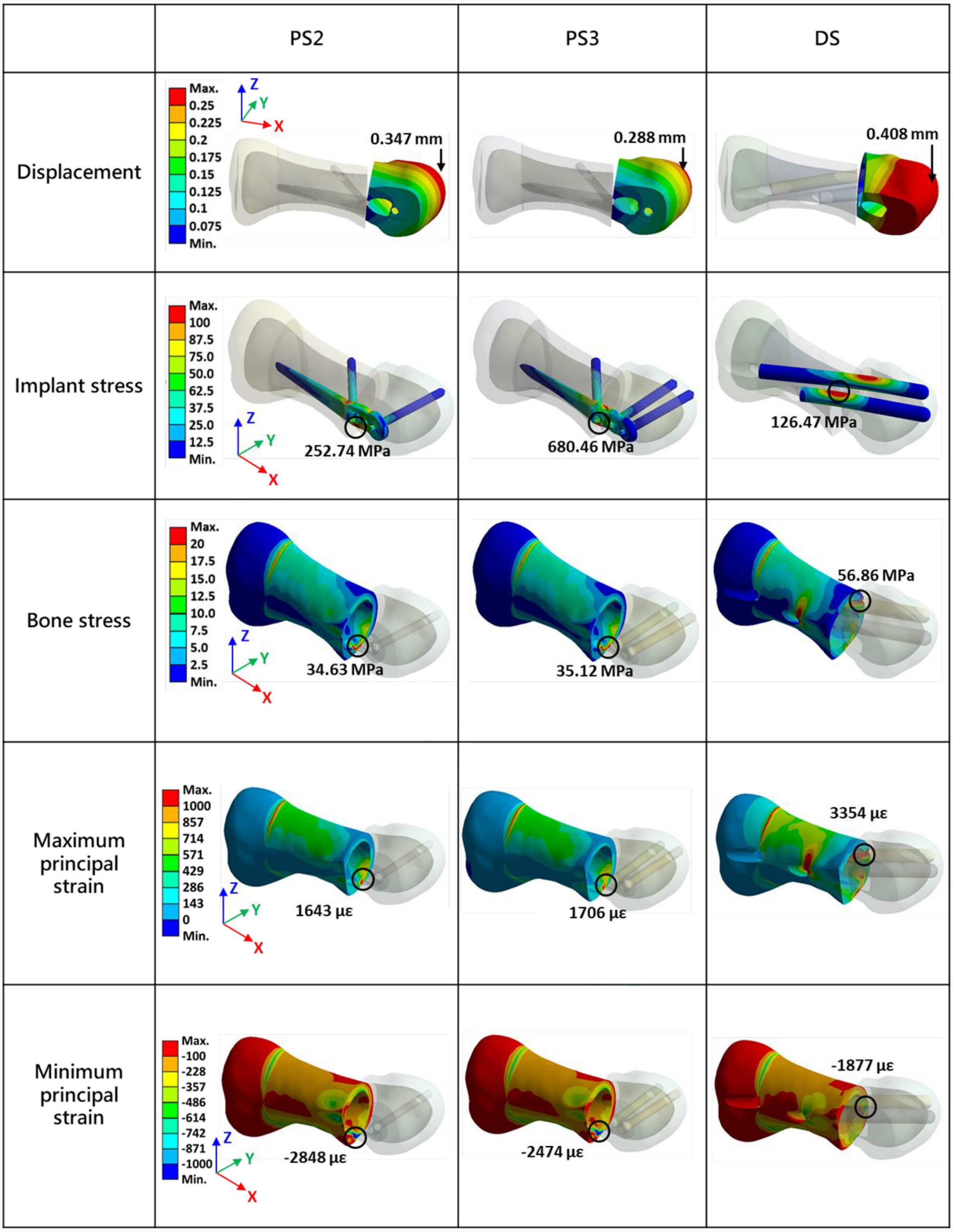

Fig. 4

Finite element analysis results under bending load conditions. Contour plots showing total displacement, von Mises stress, and maximum/minimum principal strain distribution in the three fixation configurations (PS2, PS3, and DS) under simulated bending loads. Mini-plate fixation demonstrates reduced osteotomy displacement and lower bone stress/strain compared with dual-screw fixation. DS, dual-screw fixation; PS2, mini-plate fixation with two locking screws; PS3, mini-plate fixation with three locking screws.

minimally invasive hallux valgus corrective surgery. Systematic reviews have demonstrated that, although two-screw fixation is generally effective in maintaining osteotomy correction and achieving satisfactory clinical outcomes, the reported results across studies remain inconsistent.[1-7] Surgical technique and screw placement have been identified as critical factors

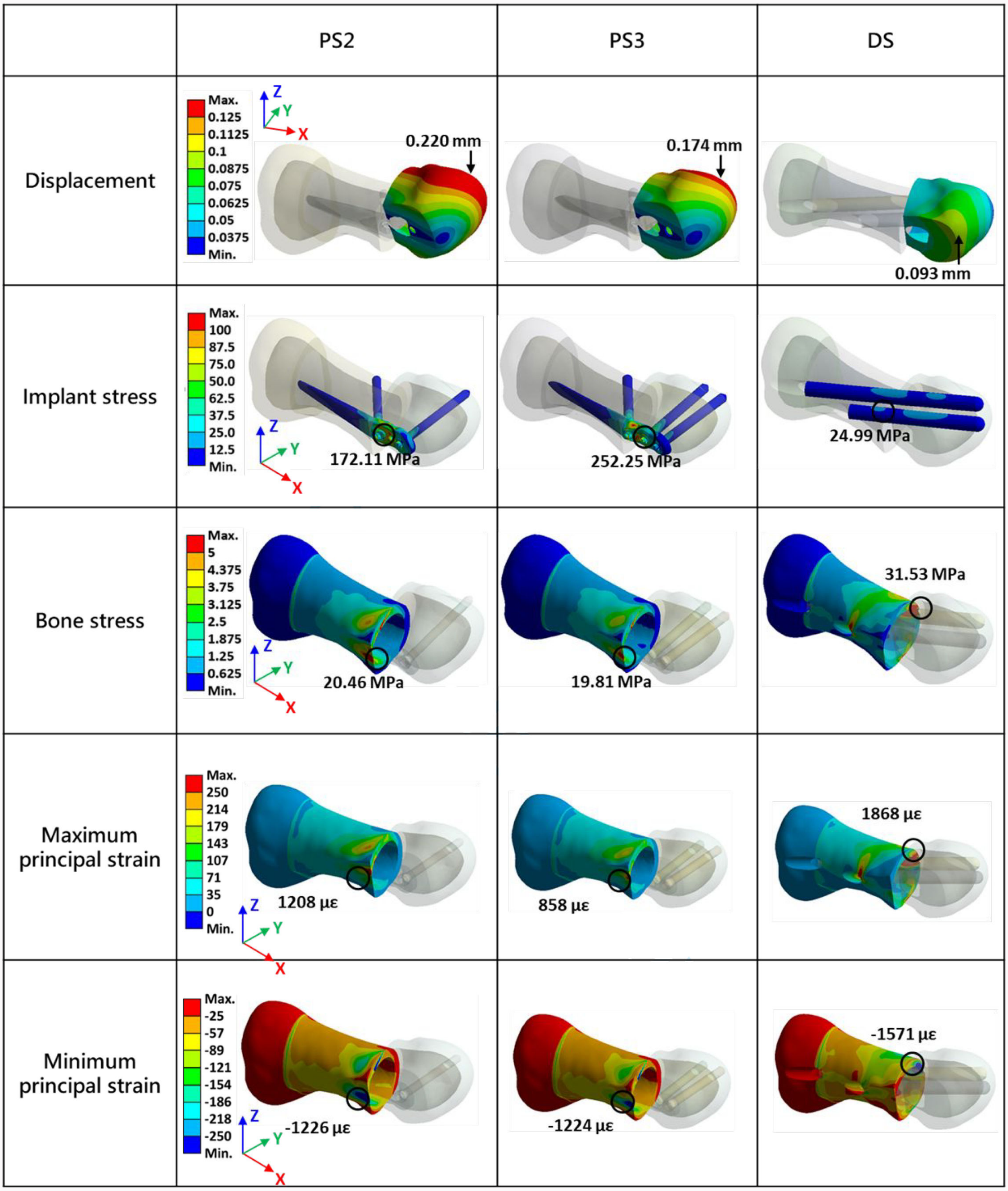

Fig. 5

Finite element analysis results under torsional load conditions. Displacement, stress, and strain distribution contours of the three fixation configurations under pure axial torsional loading. Dual-screw fixation exhibits lower overall displacement, whereas higher stress/strain concentrations are observed in bone tissue compared with in mini-plate fixation. DS, dual-screw fixation; PS2, mini-plate fixation with two locking screws; PS3, mini-plate fixation with three locking screws.

influencing postoperative outcomes.[33] Biomechanical and FE studies further indicate that screw orientation and positioning substantially affect stress distribution and micromotion at the osteotomy interface.[19,22,26,27,30,33,34]

Accordingly, the present study combined FEA with cadaveric testing to compare three fixation strategies. FEA enables the simulation of loading conditions that are difficult to reproduce experimentally, such as pure torsion, and allows evaluation of internal stress and strain distributions that cannot be directly measured, thereby providing mechanistic insights into the observed biomechanical behaviour. Under bending loading, the FE model predicted that PS3 exhibited

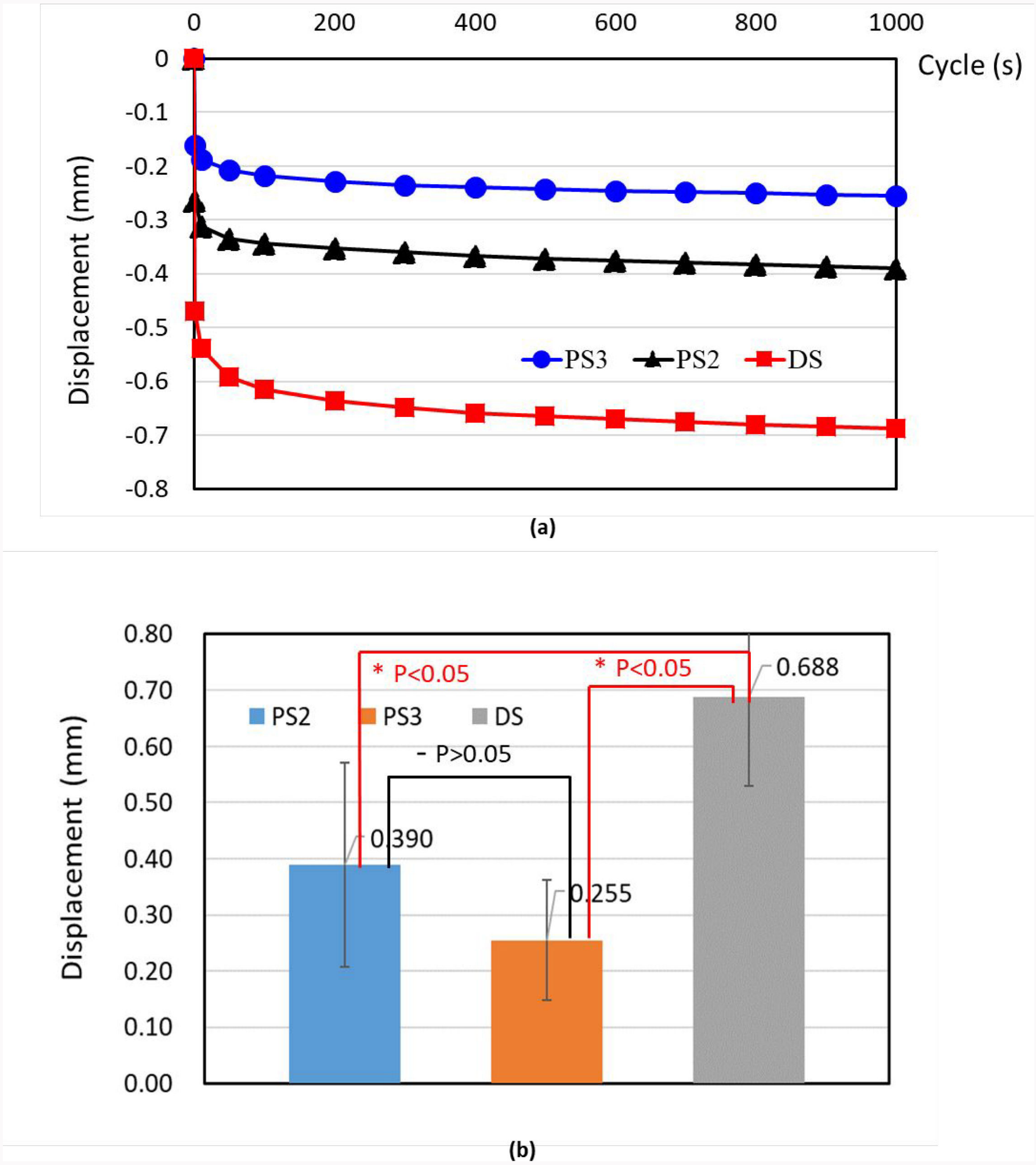

Fig. 6

Cyclic bending test displacement outcomes. a) Mean first metatarsal head displacement plotted against cycle number (0 to 1,000 cycles) under cyclic bending loading for PS2, PS3, and DS. Each curve represents the group mean (n = 3 per fixation strategy). b) Comparison of mean first metatarsal head displacement at 1,000 cycles among PS2, PS3, and DS. Error bars indicate variability within each group (n = 3). Statistical significance is denoted as shown ($p < 0.05$; not significant, $p > 0.05$). DS, dual-screw fixation; PS2, mini-plate fixation with two locking screws; PS3, mini-plate fixation with three locking screws.

the smallest displacement (0.288 mm), followed by PS2 (0.347 mm), whereas DS showed the largest displacement (0.408 mm). From a bone stress- and strain-based perspective, both the von Mises stress and the ε_1 followed the trend DS > PS3 > PS2. The ε_1 value of DS exceeded the commonly reported physiological strain range associated with bone formation (~1,000 $\mu\varepsilon$ to ~3,000 $\mu\varepsilon$), suggesting an increased risk of localized microdamage.[35-40] In contrast, PS2 and PS3 remained within this range, indicating a more favourable mechanical environment for bone maintenance and remodelling. Meanwhile, the more negative ε_3 observed in PS2 and PS3 indicates enhanced compressive load sharing, which is generally better tolerated by trabecular bone and may reduce the risk of tensile-driven failure.

A similar displacement trend was observed experimentally after 1,000 cycles (PS3: 0.255 mm; PS2: 0.390 mm; DS:

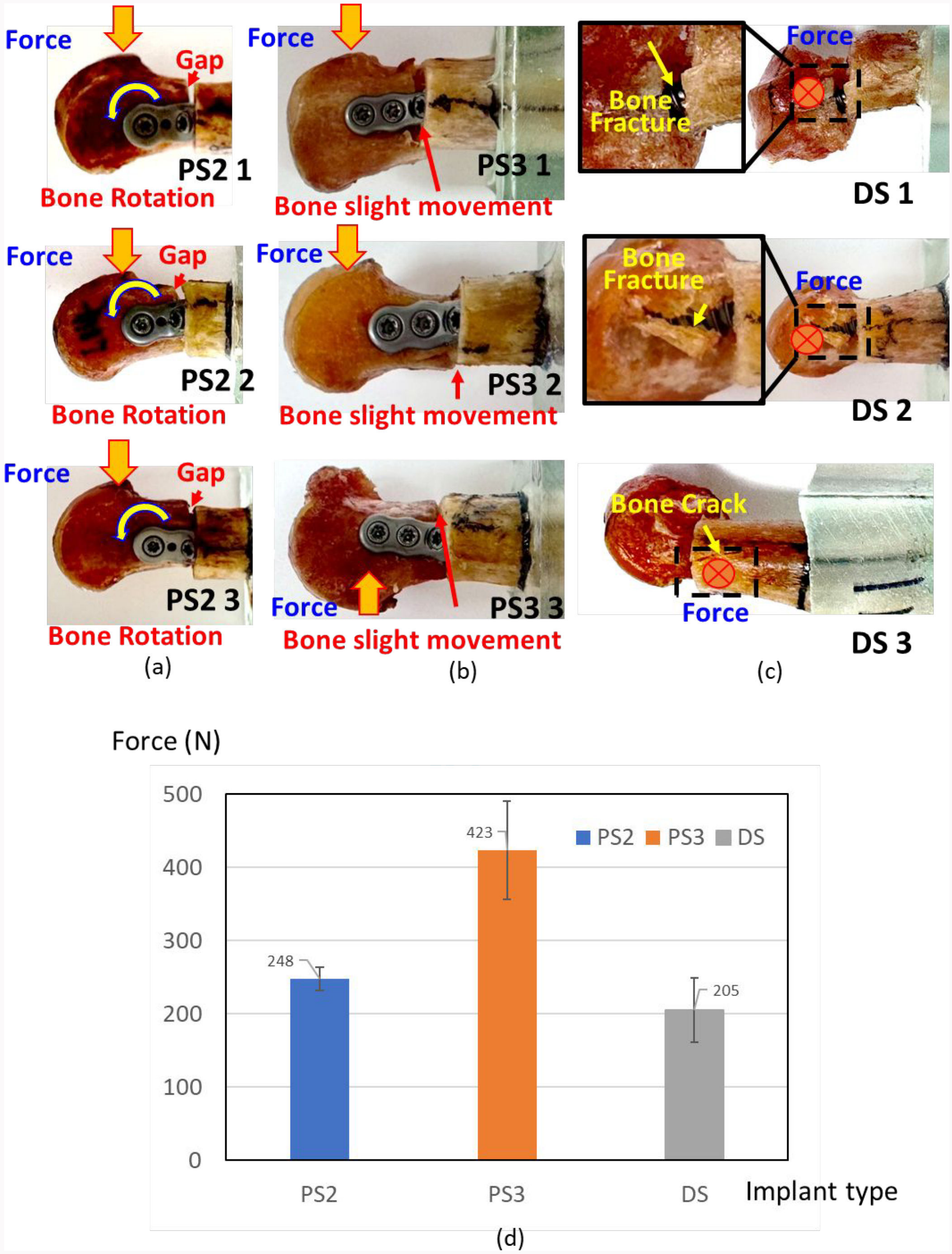

Fig. 7

a) Representative failure modes of the PS2 fixation construct showing bone rotation and gap opening at the osteotomy site under static compressive loading. b) Representative failure modes of the PS3 fixation construct showing only slight bone movement with preserved osteotomy contact. c) Representative failure modes of the DS fixation construct characterized by bone fracture or crack adjacent to the osteotomy site. d) Comparison of maximum failure loads among the three fixation groups, demonstrating the highest load-bearing capacity in the PS3 group. DS, dual-screw fixation; PS2, mini-plate fixation with two locking screws; PS3, mini-plate fixation with three locking screws.

0.688 mm). The consistent ranking between the FE results under bending and the experimental findings supports the predictive capability of the FE model in capturing relative mechanical behaviour under primary loading conditions, despite simplified material assumptions.

The biomechanical cyclic bending results represent one of the most clinically relevant findings of this study.

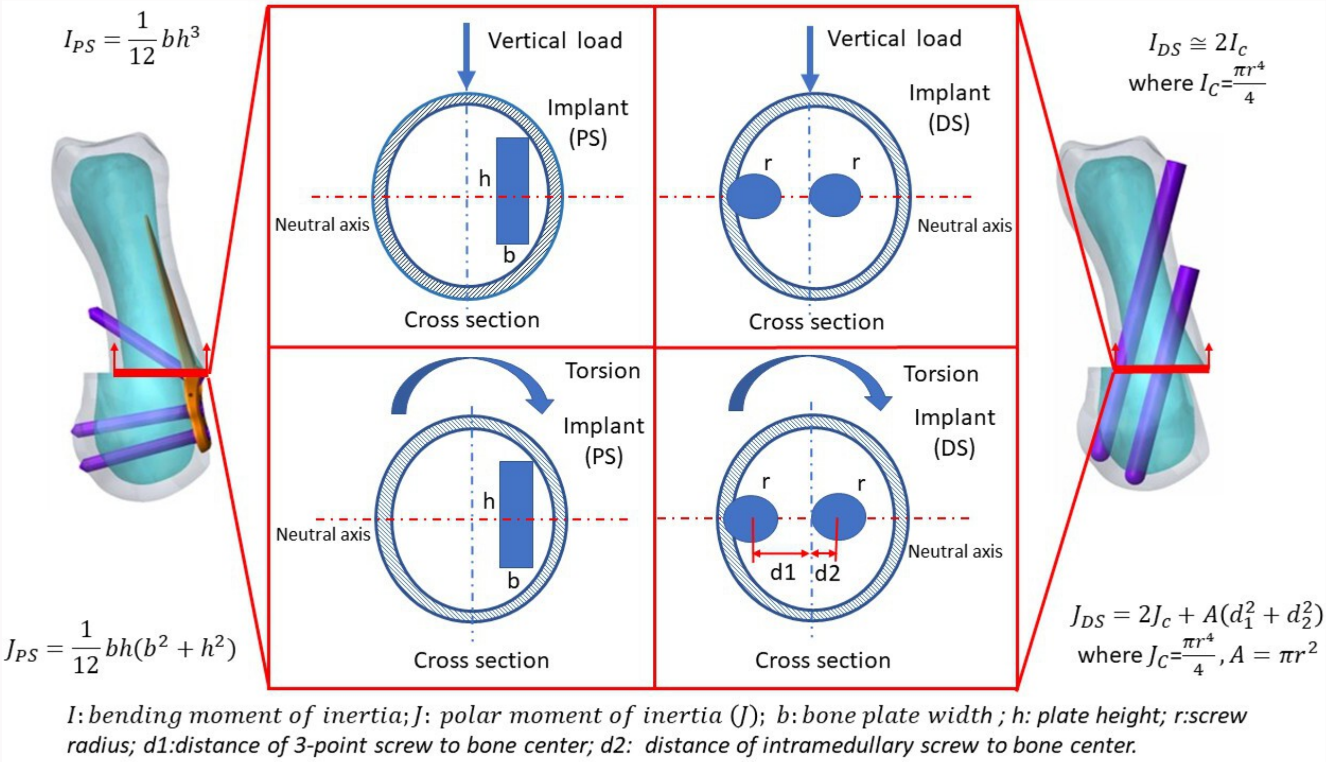

Fig. 8

Structural mechanics illustration and theoretical comparison of bending and torsional resistance between mini-plate (PS) and dual-screw (DS) fixation. Schematic diagrams illustrate the geometrical distribution of material relative to the neutral axis under bending (upper row) and torsional loading (lower row) for PS fixation (left) and DS fixation (right). For bending-dominated loading, the mini-plate configuration positions material farther from the neutral axis, resulting in a larger second moment of inertia (*I*) compared with the dual-screw configuration. For pure torsional loading, the dual-screw configuration increases the polar moment of inertia (*J*) by distributing material on opposite sides of the neutral axis.

All constructs exhibited an initial increase in displacement followed by stabilization; however, the DS configuration showed continuous displacement accumulation, whereas PS2 and PS3 demonstrated improved control of micromotion. PS3 exhibited the lowest displacement throughout cyclic loading. Given the established association between excessive micromotion and fixation failure, these findings highlight the importance of bending stability during early postoperative weightbearing.

From a biomechanical perspective, these findings align with the predominance of sagittal-plane bending loads acting on the first metatarsal during gait.[20,25] Accordingly, resistance to bending-induced micromotion should be considered a key mechanical criterion when evaluating fixation strategies for MIS distal metatarsal osteotomy. As illustrated in Figure 8, structural mechanics concepts – specifically the second moment of inertia (*I*) and the polar moment of inertia (*J*) – explain the observed mechanical differences. Under bending loading, the mini-plate configuration increases *I* by distributing material farther from the neutral axis.[28,32] In contrast, the DS construct concentrates material near the neutral axis. Under torsional loading, the DS configuration increases *J*, explaining its lower displacement under idealized torsion. However, torsional loading should be interpreted cautiously, as the first metatarsal is rarely subjected to isolated torsion during normal activities.

Based on the findings of this study, mini-plate fixation facilitated load transfer from bone to implant, reducing bone stress while increasing implant stress.[24,31] This redistribution may reduce stress concentration in bone and could be beneficial in compromised bone conditions or early weight-bearing scenarios. Mini-plate fixation may also offer practical advantages by simplifying implantation and reducing reliance on precise screw positioning compared with DS fixation.[20,23]

In addition, the loading conditions in this study were designed to provide standardized and relatively demanding scenarios rather than exact physiological replication. In the cadaveric experiments, cyclic loading (~ 31 N) was defined based on previous literature and clinical relevance, corresponding to approximately one-third of the failure load.[12,19,27] In contrast, a higher load (100 N) was applied in the FEA to represent a more conservative condition and to enhance differentiation among fixation strategies. For torsional loading, due to the lack of well-established in vivo data for the first metatarsal, the applied moment (500 N/mm) was estimated using a simplified mechanical assumption based on the bending load magnitude (50 N = half of bending load) and an approximate metatarsal radius (10 mm). Accordingly, the selected loading conditions should be interpreted as controlled comparative scenarios rather than exact physiological values.

Several limitations should be acknowledged. First, the FE model employed linear elastic material properties and did not incorporate time-dependent or non-linear behaviours such as fatigue or creep; therefore, it cannot simulate long-term cyclic degradation. However, the consistency between FE predictions and experimental results suggests that the model is sufficient to capture early-stage mechanical behaviour. Second, the model included only the first metatarsal and did not account for the metatarsophalangeal and tarsometatarsal joints, ligaments, or tendons, and therefore does not fully represent the biomechanics of the entire foot. Third, the cadaver biomechanical testing was limited to bending loading and could not reproduce isolated torsional loading in physical specimens, primarily due to practical constraints related to experimental setup and specimen fixation. In addition, the osteotomy displacement and screw configurations evaluated in this study were standardized and did not account for variability in correction magnitude or bone quality across different patient populations.

Future studies may incorporate multidirectional dynamic loading simulations or alternative bone conditions, such as osteoporotic models, to better reflect clinical variability. Furthermore, integration of clinical follow-up data – assessing long-term outcomes such as maintenance of correction, pain relief, and complication rates – would further validate the mechanical findings of this study and support the clinical translation of mini-plate fixation strategies.

References

1. **Malagelada F**, **Sahirad C**, **Dalmau-Pastor M**, **et al**. Minimally invasive surgery for hallux valgus: a systematic review of current surgical techniques. *Int Orthop*. 2019;43(3):625–637.
2. **Alimy A-R**, **Polzer H**, **Ocokoljic A**, **et al**. Does minimally invasive surgery provide better clinical or radiographic outcomes than open surgery in the treatment of hallux valgus deformity? A systematic review and meta-analysis. *Clin Orthop Relat Res*. 2023;481(6):1143–1155.
3. **Ji L**, **Wang K**, **Ding S**, **Sun C**, **Sun S**, **Zhang M**. Minimally invasive vs. open surgery for hallux valgus: a meta-analysis. *Front Surg*. 2022; 9:843410.
4. **Del Vecchio JJ**, **Ghioldi ME**. Evolution of minimally invasive surgery in hallux valgus. *Foot Ankle Clin*. 2020;25(1):79–95.
5. **Lewis TL**, **See A**, **Thomas M**, **et al**. The inaugural UK national hallux valgus think tank: identification of key issues and strategies to improve clinical care for patient benefit. *Bone Jt Open*. 2025;6(4):432–439.
6. **Lewis TL**, **Barakat A**, **Mangwani J**, **Ramasamy A**, **Ray R**. Current concepts of fourth-generation minimally invasive and open hallux valgus surgery. *Bone Joint J*. 2025;107-B(1):10–18.
7. **Lewis TL**, **Ray R**, **Miller G**, **Gordon DJ**. Third-generation minimally invasive chevron and Akin osteotomies (MICA) in hallux valgus surgery: two-year follow-up of 292 cases. *J Bone Joint Surg Am*. 2021;103-A(13): 1203–1211.
8. **Tay AYW**, **Goh GS**, **Koo K**, **Yeo NEM**. Third-generation minimally invasive chevron-Akin osteotomy for hallux valgus produces similar clinical and radiological outcomes as scarf-Akin osteotomy at 2 years: a matched cohort study. *Foot Ankle Int*. 2022;43(3):321–330.
9. **Lai MC**, **Rikhraj IS**, **Woo YL**, **Yeo W**, **Ng YCS**, **Koo K**. Clinical and radiological outcomes comparing percutaneous chevron-Akin osteotomies vs open scarf-Akin osteotomies for hallux valgus. *Foot Ankle Int*. 2018;39(3):311–317.
10. **Redfern D**, **Vernois J**. Minimally invasive chevron Akin (MICA) for correction of hallux valgus. *Tech Foot Ankle Surg*. 2016;15(1):3–11.
11. **Lewis TL**, **Robinson PW**, **Ray R**, **et al**. Five-year follow-up of third-generation Percutaneous Chevron and Akin Osteotomies (PECA) for hallux valgus. *Foot Ankle Int*. 2023;44(2):104–117.
12. **So Tamil Selven D**, **Shajahan Mohamed Buhary K**, **Yew A**, **Kumarsing Ramruttun A**, **Tay KS**, **Eng Meng Yeo N**. Biomechanical consequences of proximal screw placement in minimally invasive surgery for hallux valgus correction. *J Foot Ankle Surg*. 2024;63(6):672–679.
13. **Kim HJ**, **Shin GJ**, **Yeo ED**, **Park YH**, **Suh DH**, **Choi GW**. Two techniques of transarticular distal soft-tissue release combined with distal chevron osteotomy for hallux valgus: a prospective randomized study. *Bone Joint J*. 2025;107-B(11):1196–1202.
14. **Harrasser N**, **Hinterwimmer F**, **Baumbach SF**, **et al**. The distal metatarsal screw is not always necessary in third-generation MICA: a case-control study. *Arch Orthop Trauma Surg*. 2023;143(8):4633–4639.
15. **Li X**, **Zhang J**, **Fu S**, **Wang C**, **Yang F**, **Shi Z**. First metatarsal single-screw minimally invasive chevron-Akin osteotomy: a cost effective and clinically reliable technique. *Front Surg*. 2022;9:1047168.
16. **Goodall R**, **Borsky K**, **Harrison CJ**, **Welck M**, **Malhotra K**, **Rodrigues JN**. Structural validation of the Manchester-Oxford Foot questionnaire for use in foot and ankle surgery. *Bone Joint J*. 2024;106-B(3):256–261.
17. **Neufeld SK**, **Dean D**, **Hussaini S**. Outcomes and surgical strategies of minimally invasive chevron/Akin procedures. *Foot Ankle Int*. 2021;42(6): 676–688.
18. **Robinson PW**, **Lam P**. Percutaneous correction of mild to severe hallux valgus deformity: the evolution and current concepts of the PECA technique. In: Cazeau C, Stiglitz Y, eds. *Percutaneous and Minimally Invasive Foot Surgery*. Cham: Springer, 2023: 101–123.
19. **Schuh R**, **Hofstaetter JG**, **Benca E**, **et al**. Biomechanical analysis of two fixation methods for proximal chevron osteotomy of the first metatarsal. *Int Orthop*. 2014;38(5):983–989.
20. **Kim JS**, **Cho HK**, **Young KW**, **Kim JS**, **Lee KT**. Biomechanical comparison study of three fixation methods for proximal chevron osteotomy of the first metatarsal in hallux valgus. *Clin Orthop Surg*. 2017;9(4):514–520.
21. **Wu DY**, **Lam EKF**. Revisiting the radiological signs for the first metatarsal pronation assessment. *Bone Jt Open*. 2024;5(11):1037–1040.
22. **Tripon M**, **Lalevee M**, **van Rooij F**, **Agu C**, **Saffarini M**, **Beaudet P**. Comparison of fore- and midfoot angles using 3DCT in standard weightbearing and sesamoid view position in feet with hallux valgus. *Bone Joint Res*. 2025;14(2):69–76.
23. **Chen KJ**, **Wang CY**, **Chiang CC**, **Wang CS**, **Chen CH**, **Yang TC**. A new technique for severe hallux valgus: mid-shaft chevron osteotomy with spear plate fixation - a retrospective case series. *J Orthop Surg Res*. 2025;20(1):874.
24. **Guo J**, **Wang L**, **Mao R**, **Chang C**, **Wen J**, **Fan Y**. Biomechanical evaluation of the first ray in pre-/post-operative hallux valgus: a comparative study. *Clin Biomech (Bristol)*. 2018;60:1–8.
25. **Wong DWC**, **Zhang M**, **Yu J**, **Leung AKL**. Biomechanics of first ray hypermobility: an investigation on joint force during walking using finite element analysis. *Med Eng Phys*. 2014;36(11):1388–1393.
26. **Mao R**, **Guo J**, **Luo C**, **Fan Y**, **Wen J**, **Wang L**. Biomechanical study on surgical fixation methods for minimally invasive treatment of hallux valgus. *Med Eng Phys*. 2017;46:21–26.
27. **Aiyer A**, **Massel DH**, **Siddiqui N**, **Acevedo JI**. Biomechanical comparison of 2 common techniques of minimally invasive hallux valgus correction. *Foot Ankle Int*. 2021;42(3):373–380.
28. **Zhang Y**, **Awrejcewicz J**, **Szymanowska O**, **et al**. Effects of severe hallux valgus on metatarsal stress and the metatarsophalangeal loading during balanced standing: a finite element analysis. *Comput Biol Med*. 2018;97:1–7.
29. **Guha I**, **Zhang X**, **Rajapakse CS**, **Chang G**, **Saha PK**. Finite element analysis of trabecular bone microstructure using CT imaging and continuum mechanical modeling. *Med Phys*. 2022;49(6):3886–3899.
30. **Xie Q**, **Li X**, **Wang P**. Three dimensional finite element analysis of biomechanics of osteotomy ends with three different fixation methods after hallux valgus minimally invasive osteotomy. *J Orthop Surg (Hong Kong)*. 2023;31(2):10225536231175235.
31. **Scott AT**, **DeOrio JK**, **Montijo HE**, **Glisson RR**. Biomechanical comparison of hallux valgus correction using the proximal chevron osteotomy fixed with a medial locking plate and the Ludloff osteotomy fixed with two screws. *Clin Biomech (Bristol)*. 2010;25(3):271–276.
32. **Reddy SC**, **Schipper ON**, **Li J**. Biomechanical evaluation of fourth generation minimally invasive distal first metatarsal osteotomy: Akin osteotomy technique on first ray articular contact properties. *Foot Ankle Spec*. 2024;17(4):406–416.
33. **Lewis TL**, **Fletcher L**, **Vulcano E**, **et al**. One versus two screw fixation in minimally invasive hallux valgus surgery: a systematic review. *Cureus*. 2025;17(11):e97907.
34. **Unal AM**, **Baran O**, **Uzun B**, **Turan AC**. Comparison of screw-fixation stabilities of first metatarsal shaft osteotomies: a biomechanical study. *Acta Orthop Traumatol Turc*. 2010;44(1):70–75.

35. **Schulte FA**, **Ruffoni D**, **Lambers FM**, **et al**. Local mechanical stimuli regulate bone formation and resorption in mice at the tissue level. *PLoS One*. 2013;8(4):e62172.
36. **De Souza RL**, **Matsuura M**, **Eckstein F**, **Rawlinson SCF**, **Lanyon LE**, **Pitsillides AA**. Non-invasive axial loading of mouse tibiae increases cortical bone formation and modifies trabecular organization: a new model to study cortical and cancellous compartments in a single loaded element. *Bone*. 2005;37(6):810–818.
37. **Lewis KJ**, **Frikha-Benayed D**, **Louie J**, **et al**. Osteocyte calcium signals encode strain magnitude and loading frequency in vivo. *Proc Natl Acad Sci USA*. 2017;114(44):11775–11780.
38. **Silva MJ**, **Brodt MD**, **Lynch MA**, **Stephens AL**, **Wood DJ**, **Civitelli R**. Tibial loading increases osteogenic gene expression and cortical bone volume in mature and middle-aged mice. *PLoS One*. 2012;7(4):e34980.
39. **Cullen DM**, **Smith RT**, **Akhter MP**. Time course for bone formation with long-term external mechanical loading. *J Appl Physiol (1985)*. 2000;88(6): 1943–1948.
40. **Aido M**, **Kerschnitzki M**, **Hoerth R**, **et al**. Effect of in vivo loading on bone composition varies with animal age. *Exp Gerontol*. 2015;63:48–58.

Author information

Y-H. Chan, MS, PhD Student,
Department of Biomedical Engineering, National Yang Ming Chaio Tung University, Taipei, Taiwan.

Y-Y. Chen, MD, PhD, Orthopaedic Surgeon
C-H. Chu, MD, MPH, Orthopaedic Surgeon
Orthopedic Department, Show-Chwan Memorial Hospital, Chang Hua, Taiwan.

K-W. Chong, MD, Orthopaedic Surgeon, BJIOS Orthopaedics, Singapore, Singapore.

H-W. Wang, PhD, Doctoral Researcher
S-F. Huang, PhD, Doctoral Researcher
C-L. Lin, PhD, Professor
Department of Biomedical Engineering, National Yang Ming Chaio Tung University, Taipei, Taiwan; Medical Device Innovation and Translation Center, National Yang Ming Chaio Tung University, Taipei, Taiwan.

Author contributions

Y-H. Chan: Conceptualization, Data curation, Methodology, Software, Writing – original draft.
Y-Y. Chen: Data curation, Methodology, Validation, Writing – original draft.
K-W. Chong: Data curation, Methodology, Validation, Writing – original draft.
C-H. Chu: Data curation, Methodology, Validation.
H-W. Wang: Investigation, Methodology.
S-F. Huang: Investigation, Methodology.
C-L. Lin: Conceptualization, Writing – original draft, Writing – review & editing.

Y-H. Chan and Y-Y. Chen contributed equally to this work.

Y-H. Chan and Y-Y. Chen are joint first authors.

Funding statement

The authors disclose receipt of the following financial or material support for the research, authorship, and/or publication of this article: this study is supported in part by NSTC project 113-2327-B-A49-001 and 114-2923-E-A49-014-MY2 Taiwan.

ICMJE COI statement

The authors have no conflicts of interest to disclose.

Data sharing

The datasets generated and analyzed in the current study are not publicly available due to data protection regulations. Access to data is limited to the researchers who have obtained permission for data processing. Further inquiries can be made to the corresponding author.

Ethical review statement

This study involved biomechanical testing using human cadaveric specimens obtained from a certified tissue supplier. All specimens were fully anonymized. The importation and use of the specimens complied with relevant regulations and were approved under an official import permit. As no living participants or identifiable personal data were involved, formal ethical approval was not required.

Open access funding

The open access fee for this article was funded by NSTC project 113-2327-B-A49-001 and 114-2923-E-A49-014-MY2 Taiwan.